MATHEMATICAL BIOSCIENCES
AND ENGINEERING
Volume **12**, Number **3**, June **2015**

doi:10.3934/mbe.2015.12.451

pp. **451–472**

A TWO OR THREE COMPARTMENTS HYPERBOLIC REACTION-DIFFUSION MODEL FOR THE AQUATIC FOOD CHAIN

Elvira Barbera, Giancarlo Consolo and Giovanna Valenti

Department of Mathematics and Computer Science, University of Messina
Viale F. Stagno D'Alcontres 31, I-98166 Messina, Italy

(Communicated by Stephen Gourley)

Abstract. Two hyperbolic reaction-diffusion models are built up in the framework of Extended Thermodynamics in order to describe the spatio-temporal interactions occurring in a two or three compartments aquatic food chain. The first model focuses on the dynamics between phytoplankton and zooplankton, whereas the second one accounts also for the nutrient. In these models, infections and influence of illumination on photosynthesis are neglected. It is assumed that the zooplankton predation follows a Holling type-III functional response, while the zooplankton mortality is linear. Owing to the hyperbolic structure of our equations, the wave processes occur at finite velocity, so that the paradox of instantaneous diffusion of biological quantities, typical of parabolic systems, is consequently removed. The character of steady states and travelling waves, together with the occurrence of Hopf bifurcations, is then discussed through linear stability analysis. The governing equations are also integrated numerically to validate the analytical results herein obtained and to extract additional information on the population dynamics.

1. **Introduction.** Most of the aquatic life is based upon plant and animal plankton communities, known as phytoplankton and zooplankton, respectively. Phytoplankton, which represents the basis of all aquatic food chains, plays a key role in ocean-atmosphere dynamics and contributes to the production of oxygen. For these reasons, the dynamics of plankton populations are widely analyzed from several points of view [6]-[7],[10],[13],[18],[22]-[24],[29],[31],[33]. Besides, since the plankton growth depends upon the availability of nutrient, several efforts are made to characterize the dynamics occurring in such two or three compartments chains [8]-[9],[14]-[16],[20],[25],[30],[32].

From the mathematical viewpoint, these dynamics are usually described through reaction-diffusion equations where the populations are gathered into compartments that usually interact mutually through prey-predator-like mechanisms. In particular, diffusion mechanisms are typically expressed through Fick-like laws which lead to parabolic models. However, such models admit an instantaneous relation between cause and effect which, in the present context, would imply the diffusion of a biological population at an infinite speed. In order to remove such an unphysical

2010 *Mathematics Subject Classification.* Primary: 35L60, 92D25, 35C07; Secondary: 35Q92.
Key words and phrases. Aquatic food chain, Hopf-bifurcation, hyperbolic reaction-diffusion model, traveling wave solutions.

effect, it is possible to build up hyperbolic reaction-diffusion equations whose derivation can be carried out by using either microscopic or macroscopic approaches (see, for instance, [17] for an excellent review on this topic). On the other hand, in the framework of a continuum description, biological phenomena are macroscopic processes which must obey thermodynamic laws, so that thermodynamics represents an efficient tool to derive possible forms of the transport equations, independently of the underlying microscopic mechanism.

Therefore, in the present work we follow the guidelines of Extended Thermodynamics [26] in order to develop hyperbolic reaction-diffusion models describing the interactions occurring in a two or three compartments aquatic food chain. Such a theory has been indeed successfully applied in many different contexts and, in particular, in biology and ecology [1]-[5],[11]-[12],[28].

In detail, the paper is organized as follows. In section 2 we build up the hyperbolic system for a basic food chain composed by phytoplankton and zooplankton only. In section 3 we generalize this two-compartments model by introducing an additional state variable representing the bottom level, the nutrient. In both sections, the stability character of steady states and travelling waves is discussed analytically and numerically. In the last section we address some concluding remarks and highlight the main differences between the two models.

2. **Hyperbolic two-compartments model.** We first consider a basic aquatic food chain consisting of two-compartments only, phytoplankton and zooplankton. In the description of this ecosystem, we make the following assumptions:

i) the ecosystem is not affected by any virus disease or infection;

ii) the influence of illumination on photosynthesis is neglected;

iii) the zooplankton predation follows a Holling type-III functional response;

iv) the zooplankton mortality is linear.

Therefore, the interaction and dispersion of phytoplankton $P(x,t)$ and zooplankton $Z(x,t)$ densities at position x and time t within an aquatic mixed layer are described through the following one-dimensional prey-predator model

$$\begin{aligned} &\tfrac{\partial P}{\partial t} + \tfrac{\partial J^P}{\partial x} = \overline{\beta}(N) P \left(1 - \tfrac{P}{\gamma}\right) - \tfrac{\lambda P^2}{\mu^2 + P^2} Z, \\ &\tfrac{\partial Z}{\partial t} + \tfrac{\partial J^Z}{\partial x} = \alpha \left(\tfrac{\lambda P^2}{\mu^2 + P^2} - \delta\right) Z, \end{aligned} \tag{1}$$

where J^P and J^Z are the dissipative fluxes; N is the nutrient density; γ is the carrying capacity of phytoplankton; the parameters λ and μ represent the maximum zooplankton grazing rate and the half-saturation constant for zooplankton grazing, respectively; α denotes the zooplankton growth efficiency and $\alpha\delta$ gives the zooplankton mortality.

Since in this section the nutrient is not considered as a field variable, we here assume that the phytoplankton growth takes the standard logistic form with a constant intrinsic growth rate $\overline{\beta}(N) = \beta$.

In order to close the system (1), the dissipative fluxes J^P and J^Z are usually assumed to satisfy a Fick-like law:

$$\begin{aligned} J^P &= -D_P \tfrac{\partial P}{\partial x}, \\ J^Z &= -D_Z \tfrac{\partial Z}{\partial x}, \end{aligned} \tag{2}$$

with constant diffusion coefficients $D_P > 0$ and $D_Z > 0$. In such a way, the model (1, 2) is in the form of a parabolic reaction-diffusion system [7, 22] which admits instantaneous diffusive effects.

To overcome this problem, we build up a hyperbolic model by means of a phenomenological approach. In detail, following the guidelines of Extended Thermodynamics [26], we consider J^P and J^Z as new field variables satisfying the following evolution equations:

$$\begin{aligned} \tfrac{\partial J^P}{\partial t} + \tfrac{\partial T^P}{\partial x} &= G^P, \\ \tfrac{\partial J^Z}{\partial t} + \tfrac{\partial T^Z}{\partial x} &= G^Z, \end{aligned} \tag{3}$$

where T^P, T^Z, G^P and G^Z must be regarded as constitutive functions of the whole set of independent variables $\left(P, Z, J^P, J^Z\right)$. The functional forms of these quantities can be restricted by considering processes close to the thermodynamic equilibrium state (characterized by vanishing $J^P$and J^Z), so that they are assumed to be linear functions of the dissipative fluxes:

$$\begin{aligned} T^P &= \zeta\left(P,Z\right) + \zeta_1\left(P,Z\right) J^P + \zeta_2\left(P,Z\right) J^Z, \\ T^Z &= \chi\left(P,Z\right) + \chi_1\left(P,Z\right) J^P + \chi_2\left(P,Z\right) J^Z, \\ G^P &= \rho\left(P,Z\right) + \rho_1\left(P,Z\right) J^P + \rho_2\left(P,Z\right) J^Z, \\ G^Z &= \nu\left(P,Z\right) + \nu_1\left(P,Z\right) J^P + \nu_2\left(P,Z\right) J^Z. \end{aligned} \tag{4}$$

The requirement that the evolution equations (3, 4) reduce to the Fick laws (2) in the stationary case leads to the following restrictions on the constitutive functions:

$$\begin{aligned} T^P &= \zeta\left(P\right), \quad G^P = -\tfrac{\zeta'(P)}{D_P} J^P, \\ T^Z &= \chi\left(Z\right), \quad G^Z = -\tfrac{\chi'(Z)}{D_Z} J^Z, \end{aligned} \tag{5}$$

where the prime stands for the derivative of the function with respect to its argument. Consequently, the evolution equations (3) become:

$$\begin{aligned} \tfrac{\partial J^P}{\partial t} + \zeta'\left(P\right) \tfrac{\partial P}{\partial x} &= -\tfrac{\zeta'(P)}{D_P} J^P, \\ \tfrac{\partial J^Z}{\partial t} + \chi'\left(Z\right) \tfrac{\partial Z}{\partial x} &= -\tfrac{\chi'(Z)}{D_Z} J^Z. \end{aligned} \tag{6}$$

A further restriction on the constitutive quantities $\zeta\left(P\right)$ and $\chi\left(Z\right)$ arises from the compatibility of the system (1, 6) with the entropy balance law:

$$\frac{\partial \eta}{\partial t} + \frac{\partial \phi}{\partial x} \geq 0, \tag{7}$$

where the concave entropy density η and the entropy flux ϕ have to be considered as constitutive functions of $\left(P, Z, J^P, J^Z\right)$. By using the Lagrange multipliers Λ, Γ, Ξ and Σ, as shown in [21], the searched compatibility is ensured if:

$$\begin{aligned} \eta &= \hat{\eta}_0\left(P\right) + \tilde{\eta}_0\left(Z\right) + \tfrac{\Xi_0(P)}{2}\left(J^P\right)^2 + \tfrac{\Sigma_0(Z)}{2}\left(J^Z\right)^2, \\ \phi &= \Lambda_0\left(P\right) J^P + \Gamma_0\left(Z\right) J^Z, \\ \Lambda &= \Lambda_0\left(P\right) + \tfrac{\Xi_0'(P)}{2}\left(J^P\right)^2, \\ \Gamma &= \Gamma_0\left(Z\right) + \tfrac{\Sigma_0'(Z)}{2}\left(J^Z\right)^2, \\ \Xi &= \Xi_0\left(P\right) J^P, \\ \Sigma &= \Sigma_0\left(Z\right) J^Z, \end{aligned} \tag{8}$$

with:

$$\begin{aligned} \hat{\eta}_0'(P) &= \Lambda_0\left(P\right), & \tilde{\eta}_0'\left(Z\right) &= \Gamma_0\left(Z\right), \\ \Lambda_0'\left(P\right) &= \Xi_0\left(P\right)\zeta'\left(P\right), & \Gamma_0'\left(Z\right) &= \Sigma_0\left(Z\right)\chi'\left(Z\right). \end{aligned} \tag{9}$$

On the other hand, the concavity condition for η with respect to the field variables leads to:

$$\Xi_0(P) < 0, \quad \Sigma_0(Z) < 0, \quad \zeta'(P) > 0, \quad \chi'(Z) > 0, \tag{10}$$

which guarantees that the relaxation times $\tau^P = D_P/\zeta'(P)$ and $\tau^Z = D_Z/\chi'(Z)$ are positive as expected and, in turn, ensures the reality of the characteristic speeds $\lambda_{1,2} = \pm\sqrt{\zeta'}$ and $\lambda_{3,4} = \pm\sqrt{\chi'}$ associated to the hyperbolic model. Moreover, as a consequence of the required concavity condition, the field equations (1, 6) are symmetric-hyperbolic in the sense of Friedrichs and Lax [19] and the Cauchy problem is well posed for suitable smooth initial data.

In the particular case $\tau^P \to 0$ and $\tau^Z \to 0$, the hyperbolic system (1, 6) reduces to the parabolic one [7, 22].

Finally, in order to reduce the number of parameters involved in our model, we rewrite the hyperbolic system so obtained in a dimensionless form by introducing the following quantities:

$$\begin{aligned} &\widehat{t} = \beta t, \qquad \widehat{x} = \tfrac{x}{L}, \qquad p = \tfrac{P}{\mu}, \qquad z = \tfrac{\lambda}{\beta\mu} Z, \quad \widehat{J}^p = \tfrac{J^P}{L\beta\mu}, \quad \widehat{J}^z = \tfrac{\lambda J^Z}{L\beta^2\mu}, \\ &\widehat{\zeta} = \tfrac{\zeta}{L^2\beta^2\mu}, \quad \widehat{\chi} = \tfrac{\lambda\chi}{L^2\beta^3\mu}, \quad d_p = \tfrac{D_P}{L^2\beta}, \quad d_z = \tfrac{D_Z}{L^2\beta}, \quad c = \tfrac{\gamma}{\mu}, \quad \widetilde{\alpha} = \tfrac{\alpha\lambda}{\beta}, \quad a = \tfrac{\delta}{\lambda}, \end{aligned} \tag{11}$$

where L is a typical length. Therefore, taking into account (11) and dropping the symbol "$\widehat{\ }$" for notation convenience, the field equations (1, 6) can be recast in vector form:

$$\mathbf{U}_t + A(\mathbf{U})\mathbf{U}_x = \mathbf{B}(\mathbf{U}), \tag{12}$$

being:

$$\mathbf{U} = \begin{pmatrix} p \\ z \\ J^p \\ J^z \end{pmatrix}, \quad A = \begin{bmatrix} 0 & 0 & 1 & 0 \\ 0 & 0 & 0 & 1 \\ \zeta' & 0 & 0 & 0 \\ 0 & \chi' & 0 & 0 \end{bmatrix}, \quad \mathbf{B} = \begin{pmatrix} g(p,z) \\ f(p,z) \\ -\frac{\zeta'}{d_p} J^p \\ -\frac{\chi'}{d_z} J^z \end{pmatrix} \tag{13}$$

and:

$$\begin{aligned} g(p,z) &= p\left(1 - \tfrac{p}{c}\right) - \tfrac{p^2}{1+p^2} z, \\ f(p,z) &= \widetilde{\alpha}\left(\tfrac{p^2}{1+p^2} - a\right) z. \end{aligned} \tag{14}$$

2.1. **Linear stability analysis.** The model (12-14) admits three spatially homogeneous equilibrium states of the form $\mathbf{U}^* = (p^*, z^*, 0, 0)$, found as solutions of the system $\mathbf{B}(\mathbf{U}) = \mathbf{0}$, that are:

i) $\mathbf{U}_1^* = (0,0,0,0)$, the trivial configuration characterizing an empty region;

ii) $\mathbf{U}_2^* = (c,0,0,0)$, the zooplankton-free configuration;

iii) $\mathbf{U}_3^* = \left(\sqrt{\tfrac{a}{1-a}}, \tfrac{p^*}{a}\left(1 - \tfrac{p^*}{c}\right), 0, 0\right)$, the coexistence state, which is meaningful iff $a < c^2/\left(1+c^2\right) = a_{cr}$.

We consider hereafter the dimensionless quantity a, accounting for both mortality and grazing of zooplankton, as the control parameter.

In order to carry out a linear stability analysis, we linearize the system (12-14) around $\mathbf{U}^*$ for small space and time dependent perturbations:

$$\mathbf{U} = \mathbf{U}^* + \tilde{\mathbf{U}} \exp\left(\omega t + i\xi x\right), \tag{15}$$

where ω and ξ are the growth factor and the wave number, respectively. Then, after inserting (15) into (12-14), the following characteristic equation for ω is obtained:

$$\left[\omega^2 - \left(g_p^* - \tfrac{\zeta'^*}{d_p}\right)\omega + \left(\xi^2 - \tfrac{g_p^*}{d_p}\right)\zeta'^*\right]\left[\omega^2 - \left(f_z^* - \tfrac{\chi'^*}{d_z}\right)\omega + \left(\xi^2 - \tfrac{f_z^*}{d_z}\right)\chi'^*\right] + \\ - \left(\omega + \tfrac{\zeta'^*}{d_p}\right)\left(\omega + \tfrac{\chi'^*}{d_z}\right) g_z^* f_p^* = 0, \tag{16}$$

being f_p^*, f_z^*, g_p^* and g_z^* the first-order partial derivatives of f and g, whereas the symbol "$*$" stands for the evaluation of the functions at $\mathbf{U}^*$.

It is straightforward to ascertain that, at the equilibria $\mathbf{U}_1^*$ and $\mathbf{U}_2^*$, the equation (16) can be factorized as follows:

$$\left[\omega^2 - \left(g_p^* - \tfrac{\zeta'^*}{d_p}\right)\omega + \left(\xi^2 - \tfrac{g_p^*}{d_p}\right)\zeta'^*\right]\left[\omega^2 - \left(f_z^* - \tfrac{\chi'^*}{d_z}\right)\omega + \left(\xi^2 - \tfrac{f_z^*}{d_z}\right)\chi'^*\right] = 0. \tag{17}$$

Therefore, under the realistic hypothesis that the dimensionless relaxations times $\tau^p = d_p/\zeta'^*$ and $\tau^z = d_z/\chi'^*$ are very small, such that $1/\tau^p \gg g_p^*$ and $1/\tau^z \gg f_z^*$, it follows that the trivial steady state $\mathbf{U}_1^*$ is always unstable, while $\mathbf{U}_2^*$ is stable for $a > a_{cr}$ where $\mathbf{U}_3^*$ is biologically meaningless.

On the other hand, the characteristic equation (16) evaluated at $\mathbf{U}_3^*$ cannot be easily factorized so that it is useful to rewrite it as:

$$\omega^4 + A_1\omega^3 + A_2\omega^2 + A_3\omega + A_4 = 0, \tag{18}$$

where, taking into account that $f_z^*|_{\mathbf{U}_3^*} = 0$, we have:

$$\begin{aligned} A_1 &= \tfrac{\zeta'^*}{d_p} + \tfrac{\chi'^*}{d_z} - g_p^*, \\ A_2 &= (\zeta'^* + \chi'^*)\,\xi^2 - g_p^*\left(\tfrac{\zeta'^*}{d_p} + \tfrac{\chi'^*}{d_z}\right) - g_z^* f_p^* + \tfrac{\zeta'^*\chi'^*}{d_p d_z}, \\ A_3 &= \left[\zeta'^*\chi'^*\left(\tfrac{1}{d_p} + \tfrac{1}{d_z}\right) - g_p^*\chi'^*\right]\xi^2 - g_z^* f_p^*\left(\tfrac{\zeta'^*}{d_p} + \tfrac{\chi'^*}{d_z}\right) - \tfrac{\zeta'^*\chi'^*}{d_p d_z} g_p^*, \\ A_4 &= \zeta'^*\chi'^*\left(\xi^4 - \tfrac{g_p^*}{d_p}\xi^2 - \tfrac{f_p^* g_z^*}{d_p d_z}\right). \end{aligned} \tag{19}$$

According to the Routh-Hurwitz criterion, the equilibrium configuration $\mathbf{U}_3^*$ is asymptotically stable iff the following inequalities are satisfied:

$$A_1 > 0, \quad A_3 > 0, \quad A_4 > 0, \quad A_1 A_2 A_3 > A_3^2 + A_1^2 A_4 \quad \forall \xi \tag{20}$$

which, taking into account that $\tau^p \ll 1$ and $\tau^z \ll 1$, lead to:

$$\begin{aligned} &\mathbf{U}_3^* \ \text{always stable} && \text{for} \quad 0 < a \le \tfrac{1}{2} \\ &\mathbf{U}_3^* \ \text{stable iff} \ \tfrac{2a}{2a-1}\sqrt{\tfrac{a}{1-a}} > c && \text{for} \quad a > \tfrac{1}{2}. \end{aligned} \tag{21}$$

Summarizing, while $\mathbf{U}_1^*$ is always unstable, the stability character of $\mathbf{U}_2^*$ and $\mathbf{U}_3^*$ depends on the value of the control parameter a. More precisely, if $a > a_{cr}$ the coexistence of the two species is forbidden and any perturbation leads to the extinction of zooplankton, namely $\mathbf{U}_2^*$ is stable. On the contrary, when $a < a_{cr}$, the inclusion of a small amount of zooplankton destabilizes $\mathbf{U}_2^*$ and the stable coexistence of phytoplankton and zooplankton is allowed iff the conditions (21) hold.

It is also easy to verify that the character of all equilibria $\mathbf{U}^*$ under uniform perturbations ($\xi = 0$) is the same as the non-uniform ones.

In order to recover more detailed information about $\mathbf{U}_3^*$, we have also studied numerically the roots of the characteristic equation (18) by using the following set of parameters [15]: $\widetilde{\alpha} = 0.5, \zeta' = \chi' = 10^5, c = 10,\ d_p = 0.06, d_z = 0.05$. For this

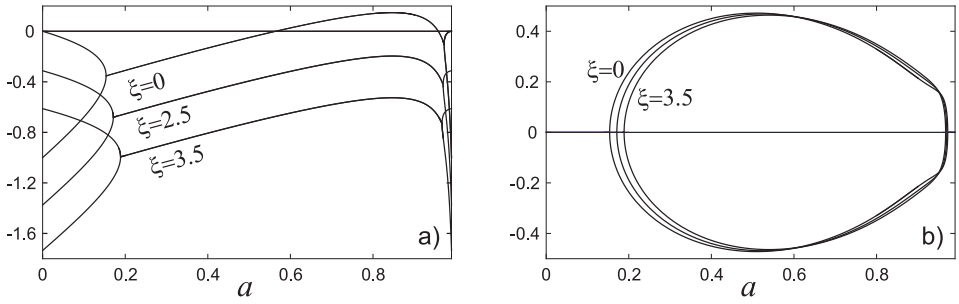

FIGURE 1. Real (left) and imaginary (right) parts of the two complex roots of eq.(18) whose character varies according to the control parameter a. In these figures, such a dependence is illustrated for both homogeneous and non-homogeneous perturbations in the range $0 \leq a \leq a_{cr} \cong 0.99$.

choice of values, we deduce that two roots are always real and negative, while the remaining ones change their character as a function of the control parameter a. In particular, in Figure 1 we show such a dependence for the real and imaginary parts of these two complex roots in the case of homogeneous ($\xi = 0$) and non-homogeneous ($\xi = 2.5$ and $\xi = 3.5$) perturbations.

From a direct inspection of Figure 1, it is possible to notice that all the roots of (18) have negative real part for $a < 0.564$ and for $a > 0.958$ whatever value of ξ. The results are in agreement with the analytical conditions given in (21) and are also consistent with those arising from the numerical integration of the field equations (12-14). In fact, in Figures 2-4 we show the numerical solutions, for three different values of a, corresponding to the following initial conditions:

$$p(x,0) = \mathrm{in}(x), \quad z(x,0) = \mathrm{in}(x), \quad J^p(x,0) = 0, \quad J^z(x,0) = 0, \tag{22}$$

where:

$$\mathrm{in}(x) = \begin{cases} 0.1 - x^2 & \text{for} \quad -\frac{1}{\sqrt{10}} < x < \frac{1}{\sqrt{10}} \\ 0 & \text{otherwise.} \end{cases} \tag{23}$$

In detail, Figure 2 ($a = 0.1$) depicts the evolution from the unstable state $\mathbf{U}_1^*$ to the stable state $\mathbf{U}_3^*$, whereas in Figure 3 ($a = 0.5$) the same transition exhibits some additional oscillations due to presence of complex eigenvalues. On the other hand, in Figure 4 ($a = 0.8$), the state $\mathbf{U}_3^*$ is unstable and the numerical results reveal the existence of a limit cycle which appears to be stable.

In all these figures it has to be noticed that the zooplankton growth is delayed with respect to the phytoplankton one. This behavior, which agrees with the one obtained in parabolic models [7, 22], is related to the choice of the smaller diffusivity for z than for p ($d_z < d_p$) and reflects the tendency of zooplankton to aggregate.

2.2. **Travelling waves.** Apart from stability analysis, information on the population dynamics can be also retrieved from the search of smooth travelling waves, namely particular solutions which travel with constant shape and connect two equilibrium states [27]. Therefore, by looking for solutions of the system (12-14) in the form $\mathbf{U} = \mathbf{U}(w)$, being $w = x - Vt$ the wave coordinate and $V > 0$ the constant

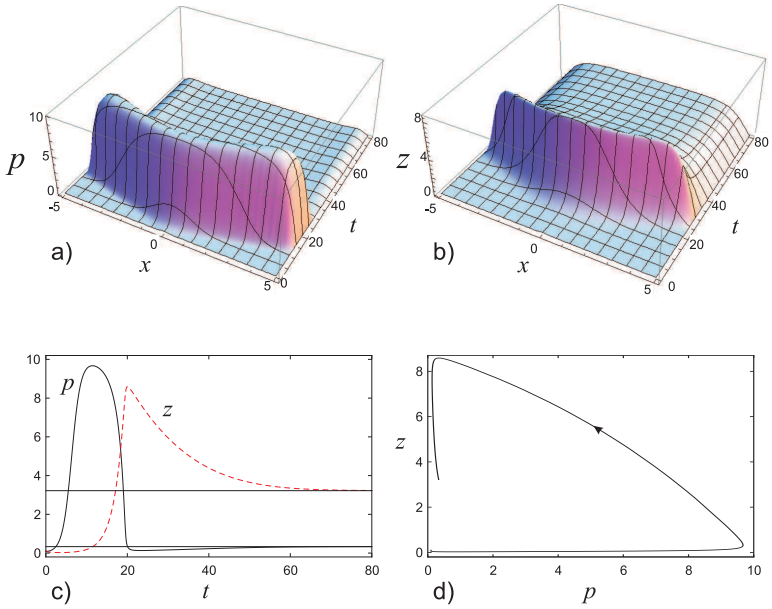

FIGURE 2. Analysis of the transition from the state $\mathbf{U}_1^*$ to the stable state $\mathbf{U}_3^*$ as a result of the numerical integration of the system (12-14) obtained by using the same parameters of Figure 1 with initial conditions (22) and $a = 0.1$. In particular, in (a),(b) we show the three-dimensional density profiles of phytoplankton and zooplankton, respectively. In (c) we plot the time evolution of these densities evaluated at $x = 0$. Here the horizontal lines are representative of the density values of the two species evaluated at $\mathbf{U}_3^*$. In (d) the parametric curve $z(p)$ depicts the transition in the phase plane.

wave speed, we obtain the following ODEs system:

$$(A - VI)\,\frac{\mathrm{d}\mathbf{U}}{\mathrm{d}w} = \mathbf{B} \tag{24}$$

with I the unit matrix.

It is straightforward to notice that system (24) admits the same steady states previously obtained. For this reason, the study of travelling wave solutions is here used to describe either the spread of zooplankton into an area where the phytoplankton has already stabilized to its carrying capacity or the spread of both species into a new environment.

As far as the character of these solutions is concerned, we linearize (24) around an homogeneous steady state $\mathbf{U}^*$ so, by introducing disturbances of the form $e^{\lambda w}$, we obtain the following characteristic equation for λ:

$$\left[\left(\zeta'^* - V^2\right)\lambda^2 - \left(g_p^* - \tfrac{\zeta'^*}{d_p}\right)V\lambda + g_p^*\tfrac{\zeta'^*}{d_p}\right]\left[\left(\chi'^* - V^2\right)\lambda^2 - \left(f_z^* - \tfrac{\chi'^*}{d_z}\right)V\lambda + f_z^*\tfrac{\chi'^*}{d_z}\right]$$
$$- \left(V\lambda - \tfrac{\zeta'^*}{d_p}\right)\left(V\lambda - \tfrac{\chi'^*}{d_z}\right)f_p^* g_z^* = 0 \tag{25}$$

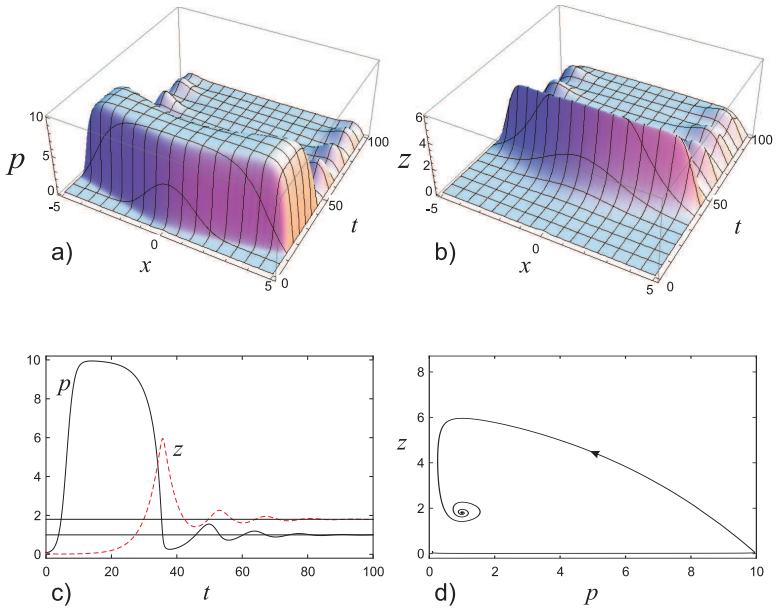

FIGURE 3. Analysis of the transition from the state $\mathbf{U}_1^*$ to the stable state $\mathbf{U}_3^*$ as a result of the numerical integration of system (12-14) obtained by using the same parameters and initial conditions of Figure 2, while the control parameter is set at $a = 0.5$. The quantities illustrated in the figures (a)-(d) are the same as the corresponding ones shown in Figure 2.

which, evaluated at $\mathbf{U}_1^*$ and $\mathbf{U}_2^*$, admits the following roots:

$$
\begin{aligned}
\lambda_{1,2}(\mathbf{U}_1^*) &= \frac{V\left(1-\frac{\zeta'^*}{d_p}\right)\pm\left[V^2\left(\frac{\zeta'^*}{d_p}+1\right)^2-4\frac{\zeta'^{*2}}{d_p}\right]^{\frac{1}{2}}}{2(\zeta'^*-V^2)},\\
\lambda_{3,4}(\mathbf{U}_1^*) &= \frac{V\left(a\tilde{\alpha}+\frac{\chi'^*}{d_z}\right)\pm\left[V^2\left(\frac{\chi'^*}{d_z}-a\tilde{\alpha}\right)^2+4\frac{a\tilde{\alpha}\chi'^{*2}}{d_z}\right]^{\frac{1}{2}}}{2(V^2-\chi'^*)},\\
\lambda_{1,2}(\mathbf{U}_2^*) &= \frac{V\left(1+\frac{\zeta'^*}{d_p}\right)\pm\left[V^2\left(\frac{\zeta'^*}{d_p}-1\right)^2+4\frac{\zeta'^{*2}}{d_p}\right]^{\frac{1}{2}}}{2(V^2-\zeta'^*)},\\
\lambda_{3,4}(\mathbf{U}_2^*) &= \frac{V\left(\tilde{\alpha}(a_{cr}-a)-\frac{\chi'^*}{d_z}\right)\pm\left[V^2\left(\frac{\chi'^*}{d_z}+\tilde{\alpha}(a_{cr}-a)\right)^2-4\tilde{\alpha}(a_{cr}-a)\frac{\chi'^{*2}}{d_z}\right]^{\frac{1}{2}}}{2(\chi'^*-V^2)}.
\end{aligned}
\tag{26}
$$

The biological requirements that p and z do not oscillate below "0" impose the following restrictions on the travelling wave speed:

$$
\begin{aligned}
&\text{at } \mathbf{U}_1^*: \quad V \geq V_1 = \frac{2\zeta'^*}{\zeta'^*+d_p}\sqrt{d_p},\\
&\text{at } \mathbf{U}_2^*: \quad V \geq V_2 = \frac{2\chi'^*}{\frac{\chi'^*}{d_z}+\tilde{\alpha}(a_{cr}-a)}\sqrt{\frac{\tilde{\alpha}}{d_z}(a_{cr}-a)} \quad \text{if} \quad a \leq a_{cr},
\end{aligned}
\tag{27}
$$

whereas no constraints apply to V at $\mathbf{U}_2^*$ if $a > a_{cr}$.

Moreover, it is easy to ascertain that, under conditions (27), both equilibria are always unstable since at least one eigenvalue is positive. Owing to the instability

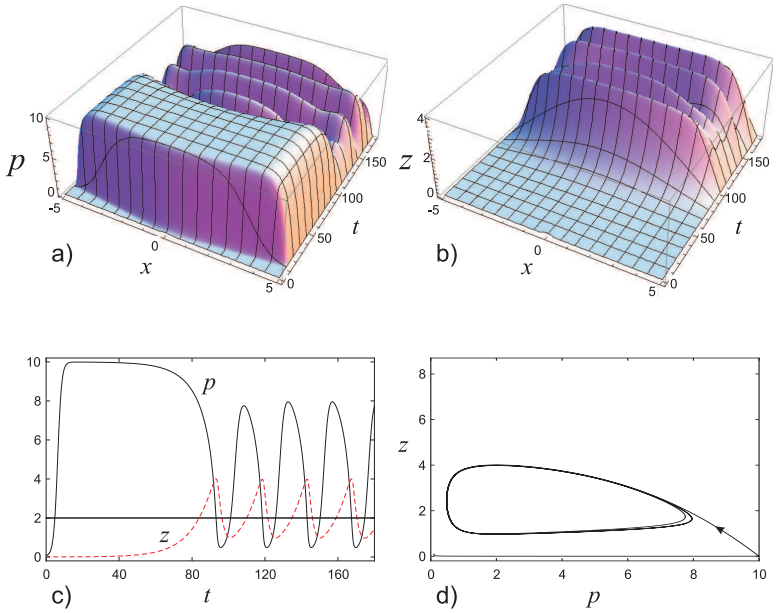

FIGURE 4. Analysis of the transition from the state $\mathbf{U}_1^*$ to a cyclic population state as a result of the numerical integration of system (12-14) obtained by using the same parameters and initial conditions of Figure 2, while the control parameter is set at $a = 0.8$. The quantities illustrated in the figures (a)-(d) are the same as the corresponding ones shown in Figure 2.

of these equilibria, we perform further investigations by considering the linearized solution of system (24) in a neighborhood of the equilibrium $\mathbf{U}_1^*$:

$$\begin{aligned} p(w) &= k_1 e^{\lambda_1 w} + k_2 e^{\lambda_2 w}, \\ z(w) &= k_3 e^{\lambda_3 w} + k_4 e^{\lambda_4 w}, \end{aligned} \tag{28}$$

with k_i $(i = 1, ..., 4)$ suitable constants depending on initial and boundary conditions. Under the restriction $V^2 < \min\{\zeta'^*, \chi'^*\}$, which is expected to take place according to the hyperbolic nature of the model, we obtain $\lambda_1 < 0$, $\lambda_2 < 0$, $\lambda_3 > 0$ and $\lambda_4 < 0$. Therefore, a travelling wave solution connecting $\mathbf{U}_1^*$ and $\mathbf{U}_2^*$ may exist if $k_3 = 0$, otherwise the corresponding linearized solution would diverge at infinite. The validation of the existence of such a connection is depicted in Figure 5, which is obtained by integrating numerically the ODEs system (24).

For what concerns the coexistence state $\mathbf{U}_3^*$, the characteristic equation (25) can be rewritten as:

$$(V\lambda)^4 + B_1 (V\lambda)^3 + B_2 (V\lambda)^2 + B_3 (V\lambda) + B_4 = 0 \tag{29}$$

with

$$B_1 = \frac{1}{\left(1-\frac{\zeta'^*}{V^2}\right)\left(1-\frac{\chi'^*}{V^2}\right)} \left[\left(\frac{\chi'^*}{V^2} - 1\right)\left(\frac{\zeta'^*}{d_p} - g_p^*\right) + \frac{\chi'^*}{d_z}\left(\frac{\zeta'^*}{V^2} - 1\right)\right],$$

$$B_2 = \frac{1}{\left(1-\frac{\zeta'^*}{V^2}\right)\left(1-\frac{\chi'^*}{V^2}\right)} \left[\frac{\zeta'^*\chi'^*}{d_p d_z} + \frac{\zeta'^*}{d_p}\left(\frac{\chi'^*}{V^2} - 1\right) g_p^* - \frac{\chi'^*}{d_z} g_p^* - f_p^* g_z^*\right],$$

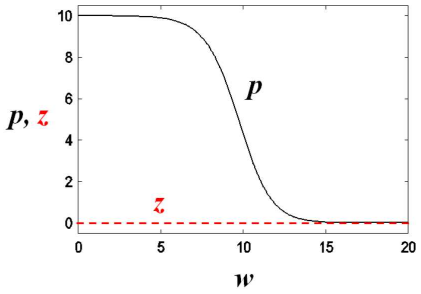

FIGURE 5. Traveling wave-like solutions connecting $\mathbf{U}_1^*$ and $\mathbf{U}_2^*$ obtained by integrating numerically the ODEs system (24) with the same parameters as those used in Figure 1 together with $a = 1.2$ and $V = 1$.

$$
\begin{aligned}
B_3 &= \frac{1}{\left(1-\frac{\zeta'^*}{V^2}\right)\left(1-\frac{\chi'^*}{V^2}\right)}\left[\left(\frac{\zeta'^*}{d_p}+\frac{\chi'^*}{d_z}\right) f_p^* g_z^* + \frac{\zeta'^*\chi'^*}{d_p d_z} g_p^*\right], \\
B_4 &= -\frac{f_p^* g_z^*}{\left(1-\frac{\zeta'^*}{V^2}\right)\left(1-\frac{\chi'^*}{V^2}\right)}\frac{\zeta'^*\chi'^*}{d_p d_z}.
\end{aligned}
\tag{30}
$$

Therefore, the stability character of $\mathbf{U}_3^*$ will be again investigated by using the Routh-Hurwitz criterion which, bearing in mind that $\zeta'^*/d_p \gg 1$ and $\chi'^*/d_z \gg 1$, is carried out by retaining the corresponding leading terms only. Moreover, taking into account the hyperbolic nature of our model, it is easy to ascertain that $B_1 > 0$ and $B_4 > 0$ are always fulfilled. The other two conditions $B_3 > 0$ and $B_1 B_2 B_3 - B_3^2 - B_1^2 B_4 > 0$ yield the following further restrictions on the control parameter and on the wave speed, respectively:

$$
\begin{aligned}
&\frac{2a}{2a-1}\sqrt{\frac{a}{1-a}} < c \quad \text{for} \quad 1/2 < a < a_{cr} \\
&\frac{a\ f_p^*\ (d_z+d_p)^2 - g_p^{*2} d_z^2}{(d_z+d_p) g_p^*} < V^2 < \min\left\{\zeta'^*, \chi'^*\right\},
\end{aligned}
\tag{31}
$$

which reveals the range of the asymptotic stability of the coexistence state $\mathbf{U}_3^*$.

Then, it is interesting to analyze whether the loss of stability of $\mathbf{U}_3^*$ gives rise to Hopf bifurcations. As known, such a bifurcation occurs under the following assumptions:
(i) the characteristic equation (29) admits a pair of purely imaginary roots and no other roots with null real part;
(ii) the transversality condition $\frac{\mathrm{d}\ \mathrm{Re}(V\lambda)}{\mathrm{d}a} \neq 0$ is fulfilled at the values of the control parameters for which the property (i) is satisfied.
In particular, the equation (29) admits two roots of the form $(V\lambda)_{1,2} = \pm i\beta$ if the following condition holds:

$$
V^2 = \frac{a\ f_p^*\ (d_z+d_p)^2 - g_p^{*2} d_z^2}{(d_z+d_p) g_p^*}.
\tag{32}
$$

Moreover, since all coefficients of (29) are real, the other two solutions $(V\lambda)_{3,4}$ can be either complex conjugate or both real. In the first case, we obtain $\mathrm{Re}(V\lambda)_{3,4} = -B_1/2 < 0$, whereas in the second one we have $(V\lambda)_3 + (V\lambda)_4 = -B_1 < 0$ and

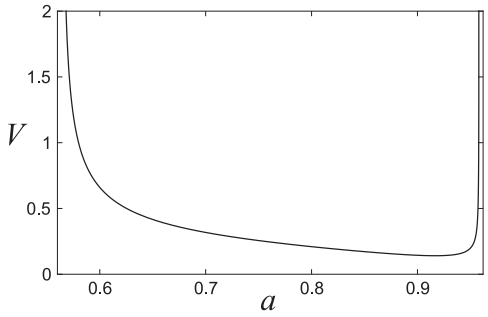

FIGURE 6. Bifurcation locus in the a-V plane. The parameters are the same used in Figure 1.

$(V\lambda)_3(V\lambda)_4 = B_1B_4/B_3 > 0$. Therefore, the real parts of these latter roots are non null and, under the condition (32), the assumption (i) is fulfilled.

On the other hand, the transversality condition (ii) reads:

$$\frac{\mathrm{d}\ \mathrm{Re}\,(V\lambda)}{\mathrm{d}a} = \frac{B_1\left(\frac{\mathrm{d}B_4}{\mathrm{d}a} - \frac{B_3}{B_1}\frac{\mathrm{d}B_2}{\mathrm{d}a}\right) + \left(B_2 - 2\frac{B_3}{B_1}\right)\left(\frac{B_3}{B_1}\frac{\mathrm{d}B_1}{\mathrm{d}a} - \frac{\mathrm{d}B_3}{\mathrm{d}a}\right)}{2\left[B_3B_1 + \left(B_2 - 2\frac{B_3}{B_1}\right)^2\right]} \neq 0 \qquad (33)$$

which, due to its complexity, has been checked and verified numerically for (a, V) satisfying (32).

Therefore, the system undergoes a Hopf bifurcation around the coexistence state $\mathbf{U}_3^*$ as a crosses the bifurcation locus represented by (32) and shown in Figure 6. In other words, at the Hopf bifurcation threshold the temporal symmetry of the system is broken and small amplitude periodic oscillations appear with frequency $\beta = V\sqrt{g_p^*/(d_p + d_z)}$. Such a threshold can be interpreted as a critical minimum value for the wave speed and, as illustrated in Figure 6, it exhibits a non monotonic dependence on the bifurcation parameter a.

In Figure 7, we show the outcome of numerical integration of the ODE system (24) obtained for $(a, V) = (0.9, 1)$, i.e. a point lying above the bifurcation locus in the phase plane. The three curves here depicted correspond to three different set of initial data (indicated by bullets), each characterized by null fluxes. As it can be noticed, the resulting unstable limit cycle (the continuous line in the figure) confirms the existence of a Hopf bifurcation, which is found to be sub-critical. From such a figure we also observe that, being $\mathbf{U}_1^*$ and $\mathbf{U}_2^*$ located outside the region defined by the limit cycle, a connection between these equilibria and the coexistence state $\mathbf{U}_3^*$ seems to be prevented.

However, the assumption typical of Extended Thermodynamics that the dissipative fluxes are independent variables allows us to obtain such a heteroclinic connection by considering non-null initial values for these field variables, as shown in Figure 8. In particular, if the system lies initially in the empty region $\mathbf{U}_1^*$, the limit cycle can be overcome and the coexistence state $\mathbf{U}_3^*$ can be achieved, as depicted by the dotted trajectory in Figure 8a. However, the system tends to diverge away from the limit cycle if the initial fluxes are slightly changed (dashed trajectory in Figure 8a), revealing a high sensitivity of the system response on the initial

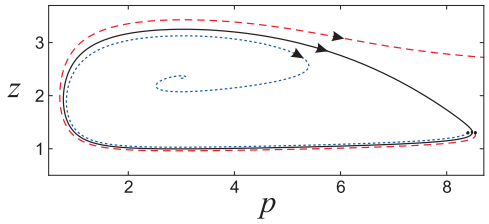

FIGURE 7. Phase plane plot of a smooth traveling wave obtained through numerical integration of the ODE system (24) with the same parameters as in Figure 1 together with $a = 0.9$ and $V = 1$. The bullets denote the three different initial data for p and z with null fluxes. Limit cycle solution (continuous line); trajectory starting near the limit cycle and spiraling slowly inwards towards the stable coexistence steady-state (dotted line); trajectory starting near the inhomogeneous limit cycle and spiraling immediately outwards far from the limit cycle solution (dashed line).

data. Analogous conclusions can be drawn if the environment is initially occupied by phytoplankton only (state $\mathbf{U}_2^*$), as shown in Figure 8b.

To the best of our knowledge, the scenario here illustrated has not been pointed out in phytoplankton-zooplankton models and could also draw the attention of biologists toward the search of this new feature.

3. **Hyperbolic three-compartments model.** The two compartments (PZ) model (12-14) previously obtained describes the interaction between zooplankton and phytoplankton under the hidden assumption that the nutrient supply is instantaneously restored. In order to establish the role of the nutrient in affecting the dynamics involved in the aquatic food web, we introduce a third compartment accounting for the nutrient density N, which is hereafter regarded as a state variable.

Therefore, in order to generalize the system (1, 2), an additional evolution equation for the nutrient has to be included and the effects of the nutrient availability on the phytoplankton growth rate have to be taken into account. The parabolic equations governing the spatially inhomogeneous interaction among these populations, proposed in [15, 30], read:

$$\begin{aligned}
&\frac{\partial N}{\partial t} + \frac{\partial J^N}{\partial x} = -\overline{\beta}(N)P\left(1 - \frac{P}{\gamma}\right) + (1-\alpha)\,\frac{\lambda P^2}{\mu^2+P^2}\,Z + S\,(N_0 - N)\,,\\
&\frac{\partial P}{\partial t} + \frac{\partial J^P}{\partial x} = \overline{\beta}(N)P\left(1 - \frac{P}{\gamma}\right) - \frac{\lambda P^2}{\mu^2+P^2}\,Z,\\
&\frac{\partial Z}{\partial t} + \frac{\partial J^Z}{\partial x} = \alpha\left(\frac{\lambda P^2}{\mu^2+P^2} - \delta\right) Z,
\end{aligned} \tag{34}$$

with

$$J^N = -D_N\frac{\partial N}{\partial x}, \quad J^P = -D_P\frac{\partial P}{\partial x}, \quad J^Z = -D_Z\frac{\partial Z}{\partial x}. \tag{35}$$

In equation $(34)_1$, J^N denotes the dissipative flux of the nutrient with $D_N > 0$, $\overline{\beta}(N) = \beta\frac{N}{K+N}$ is a Michaelis-Menten function with K the half-saturation constant, whereas the last two terms represent, respectively, the nutrient recycling from dead zooplankton and the input of nutrient to the system, being S the cross-thermocline exchange rate and N_0 the nutrient concentration below the mixed layer.

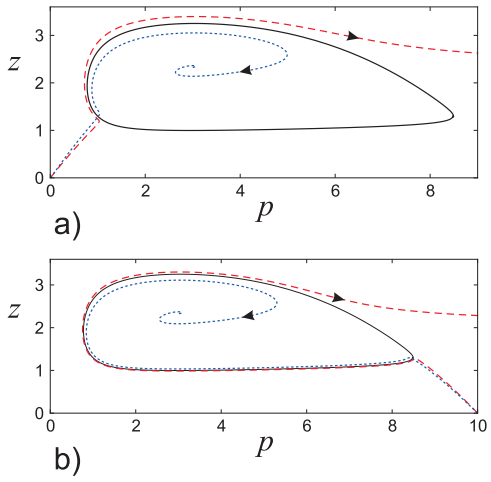

FIGURE 8. (a) Phase plane plot of heteroclinic connection between $\mathbf{U}_1^*$ and $\mathbf{U}_3^*$ obtained by using the same parameters as in Figure 7. The trajectory depicted by dotted line is obtained with the following initial conditions $(p, z, J^p, J^z) = (0.01, 0.01, -0.9, -0.93)$ whereas the one represented by dashed line corresponds to $(0.01, 0.01, -0.9, -0.92)$. The continuous curve is the limit cycle. (b) An analogous phase plane plot of heteroclinic connection between $\mathbf{U}_2^*$ and $\mathbf{U}_3^*$ obtained by using the following initial conditions $(9.99, 0.01, 0.96, -0.93)$ relatively to the dotted curve and $(9.99, 0.01, 0.95, -0.93)$ for the dashed curve.

In order to build up the corresponding hyperbolic reaction-diffusion model, we follow again the leading ideas of the Extended Thermodynamic theory already presented in the previous section. Therefore, by considering the same dimensionless quantities introduced in (11) together with the following ones:

$$n = \frac{N}{\mu}, \quad \widehat{J}^n = \frac{J^N}{L\beta\mu}, \quad k = \frac{K}{\mu}, \quad s = \frac{S}{\beta}, \quad n_0 = \frac{N_0}{\mu}, \quad d_n = \frac{D_N}{L^2\beta}, \quad \widehat{\nu} = \frac{\nu}{L^2\beta^2\mu} \tag{36}$$

the resulting governing system can be written in the vector form (12) with:

$$\mathbf{U} = \begin{pmatrix} n \\ p \\ z \\ J^n \\ J^p \\ J^z \end{pmatrix}, \quad A = \begin{bmatrix} 0 & 0 & 0 & 1 & 0 & 0 \\ 0 & 0 & 0 & 0 & 1 & 0 \\ 0 & 0 & 0 & 0 & 0 & 1 \\ \nu' & 0 & 0 & 0 & 0 & 0 \\ 0 & \zeta' & 0 & 0 & 0 & 0 \\ 0 & 0 & \chi' & 0 & 0 & 0 \end{bmatrix}, \quad \mathbf{B} = \begin{pmatrix} h(n,p,z) \\ G(n,p,z) \\ f(p,z) \\ -\frac{\nu'}{d_n} J^n \\ -\frac{\zeta'}{d_p} J^p \\ -\frac{\chi'}{d_z} J^z \end{pmatrix}. \tag{37}$$

where, for simplicity of notation, we have removed the "$\widehat{\ }$" symbol. In (37), $\tau^n = \frac{d_n}{\nu'(n)} > 0$ represents the nutrient relaxation time whereas the source terms are given

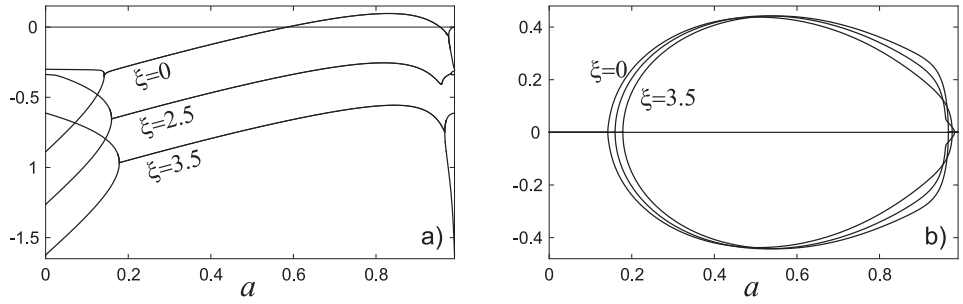

FIGURE 9. Real (left) and imaginary (right) parts of two complex roots of equation (41) versus the control parameter a.

by:

$$\begin{aligned} h(n,p,z) &= -\tfrac{n}{k+n}p\left(1-\tfrac{p}{c}\right)+(1-\alpha)\,\tfrac{p^2}{1+p^2}z+s\,(n_0-n)\,,\\ G(n,p,z) &= \tfrac{n}{k+n}p\left(1-\tfrac{p}{c}\right)-\tfrac{p^2}{1+p^2}z,\\ f(p,z) &= \widetilde{\alpha}\left(\tfrac{p^2}{1+p^2}-a\right)z. \end{aligned} \tag{38}$$

3.1. **Linear stability analysis.** The equilibrium states $\mathbf{U}^*=(n^*,p^*,z^*,0,0,0)$ of the three-compartments (NPZ) hyperbolic model in point are found to be

$$\begin{aligned} &\mathbf{U}_1^*=(n_0,0,0,0,0,0)\,,\quad \mathbf{U}_2^*=(n_0,c,0,0,0,0)\,,\\ &\mathbf{U}_3^*=\left(n^*,\sqrt{\tfrac{a}{1-a}},\tfrac{s(n_0-n^*)}{\alpha a},0,0,0\right) \end{aligned} \tag{39}$$

being

$$n^*=\frac{n_0-k-\frac{\alpha}{s}\sqrt{\frac{a}{1-a}}\left(1-\frac{1}{c}\sqrt{\frac{a}{1-a}}\right)+\sqrt{\left[n_0-k-\frac{\alpha}{s}\sqrt{\frac{a}{1-a}}\left(1-\frac{1}{c}\sqrt{\frac{a}{1-a}}\right)\right]^2+4kn_0}}{2}. \tag{40}$$

It is easy to see that the nutrient-only configuration $\mathbf{U}_1^*$ as well as the zooplankton-free one $\mathbf{U}_2^*$ always exist, whereas the coexistence state $\mathbf{U}_3^*$ is biologically relevant iff $0<a<a_{cr}$.

The linear stability analysis is carried out by seeking solutions of the form (15) and the resulting characteristic equation reads:

$$\begin{aligned} &\left[\omega^2+\left(\tfrac{\zeta'^*}{d_p}-G_p^*\right)\omega+\left(\xi^2-\tfrac{G_p^*}{d_p}\right)\zeta'^*\right]\left[\omega^2+\left(\tfrac{\nu'^*}{d_n}-h_n^*\right)\omega+\left(\xi^2-\tfrac{h_n^*}{d_n}\right)\nu'^*\right]\times\\ &\times\left[\omega^2+\left(\tfrac{\chi'^*}{d_z}-f_z^*\right)\omega+\left(\xi^2-\tfrac{f_z^*}{d_z}\right)\chi'^*\right]+\\ &-\left(\omega+\tfrac{\zeta'^*}{d_p}\right)\left(\omega+\tfrac{\nu'^*}{d_n}\right)\left[\omega^2+\left(\tfrac{\chi'^*}{d_z}-f_z^*\right)\omega+\left(\xi^2-\tfrac{f_z^*}{d_z}\right)\chi'^*\right]G_n^*h_p^*+\\ &-\left(\omega+\tfrac{\zeta'^*}{d_p}\right)\left(\omega+\tfrac{\chi'^*}{d_z}\right)\left[\omega^2+\left(\tfrac{\nu'^*}{d_n}-h_n^*\right)\omega+\left(\xi^2-\tfrac{h_n^*}{d_n}\right)\nu'^*\right]G_z^*f_p^*+\\ &-\left(\omega+\tfrac{\zeta'^*}{d_p}\right)\left(\omega+\tfrac{\nu'^*}{d_n}\right)\left(\omega+\tfrac{\chi'^*}{d_z}\right)G_n^*h_z^*f_p^*=0. \end{aligned} \tag{41}$$

Since $G_n^*|_{\mathbf{U}_{1,2}^*}=f_p^*|_{\mathbf{U}_{1,2}^*}=0$, the characteristic equation (41) can be easily factorized at $\mathbf{U}_1^*$ and $\mathbf{U}_2^*$, so we deduce that the equilibrium $\mathbf{U}_1^*$ is always unstable, while $\mathbf{U}_2^*$ is stable for $f_z^*|_{\mathbf{U}_2^*}<0$, i.e. for $a>a_{cr}$.

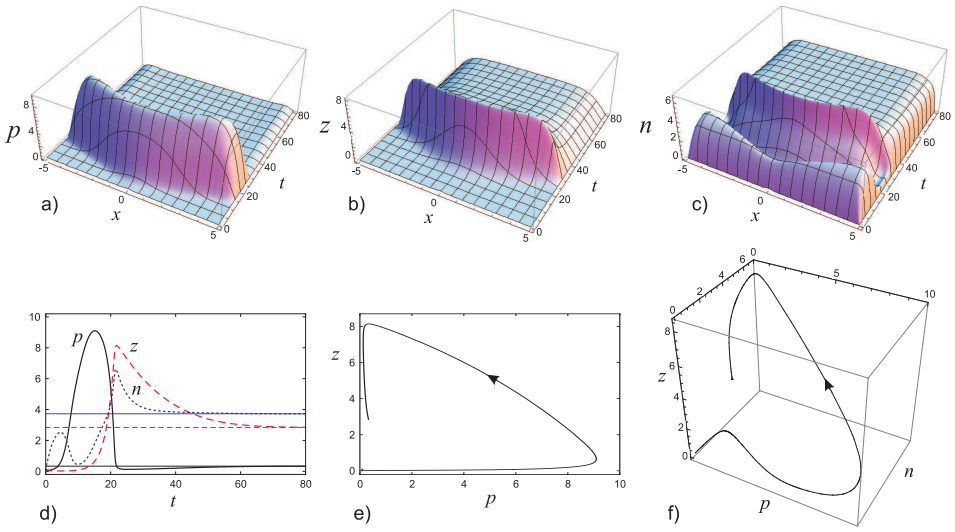

FIGURE 10. Transition from an empty region to the state $\mathbf{U}_3^*$ which is stable for $a = 0.1$. In Figures (a)-(c) the three-dimensional density profiles of phytoplankton, zooplankton and nutrient, are shown respectively. The time evolution of p, z and n at $x = 0$ is plotted in (d) being the horizontal lines the values of p, z and n evaluated at $\mathbf{U}_3^*$. The transition in the p-z phase plane is shown in (e), whereas in (f) the trajectory is depicted in the n-p-z phase space.

On the contrary, the sixth-order equation (41) evaluated at $\mathbf{U}_3^*$ is quite complex to be solved analytically and, for this reason, the corresponding linear stability analysis is carried out numerically.

In such a numerical analysis, we consider the same values of the parameters chosen in the two-compartments model together with $s = 0.3$, $k = 0.5$, $n_0 = 4$, $\nu' = 10^5, d_n = 0.006$ and $\alpha = 0.29$. By using this set of parameters, we find that four roots of (41) are always real and negative, whereas the remaining ones change their character according to the control parameter a. The dependence of the real and imaginary parts of these two complex roots is depicted in Figure 9 for homogeneous ($\xi = 0$) and non-homogeneous ($\xi = 2.5$ and $\xi = 3.5$) perturbations.

From such a figure we can deduce that the equilibrium $\mathbf{U}_3^*$ is stable for $a < 0.585 = a_1$ and $a > 0.955 = a_2$.

The dynamical properties of the model under investigation are also evaluated through a direct numerical integration of (12,37,38) by assuming null initial conditions and considering three different values of a. These solutions are shown in Figures 10-12.

More precisely, in Figures 10 ($a = 0.1$) and 11 ($a = 0.5$) the system evolves from an empty region towards the stable coexistence state $\mathbf{U}_3^*$, being $a < a_1$ in both cases. As it can be noticed, the dynamics corresponding to $a = 0.5$ exhibits additional oscillations consistent with the presence of complex eigenvalues and in agreement with the numerical results shown in Figure 9. On the contrary, the dynamics observed in Figure 12 ($a_1 < a = 0.8 < a_2$) takes place through a stable limit cycle.

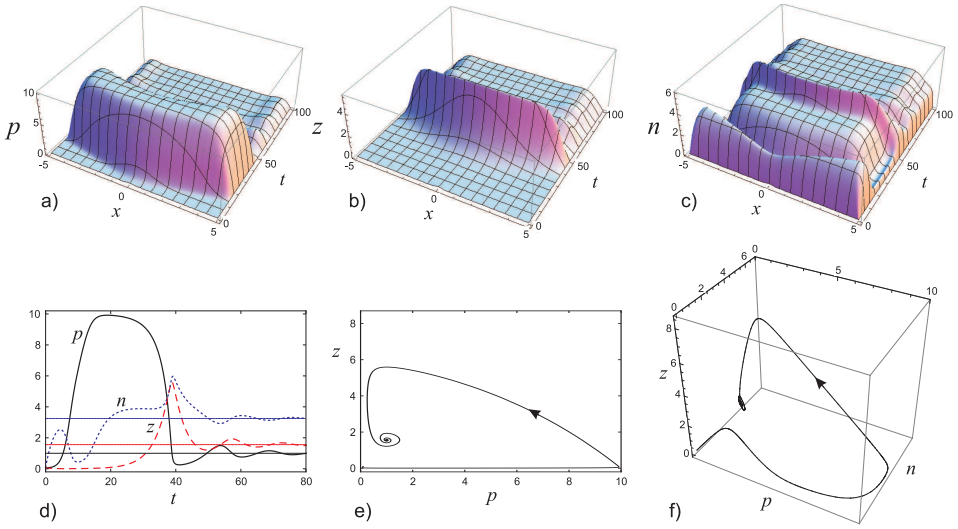

FIGURE 11. Transition from an empty region to the state $\mathbf{U}_3^*$ which is stable for $a = 0.5$. The quantities illustrated in the figures (a)-(f) are the same as the corresponding ones shown in Figure 10.

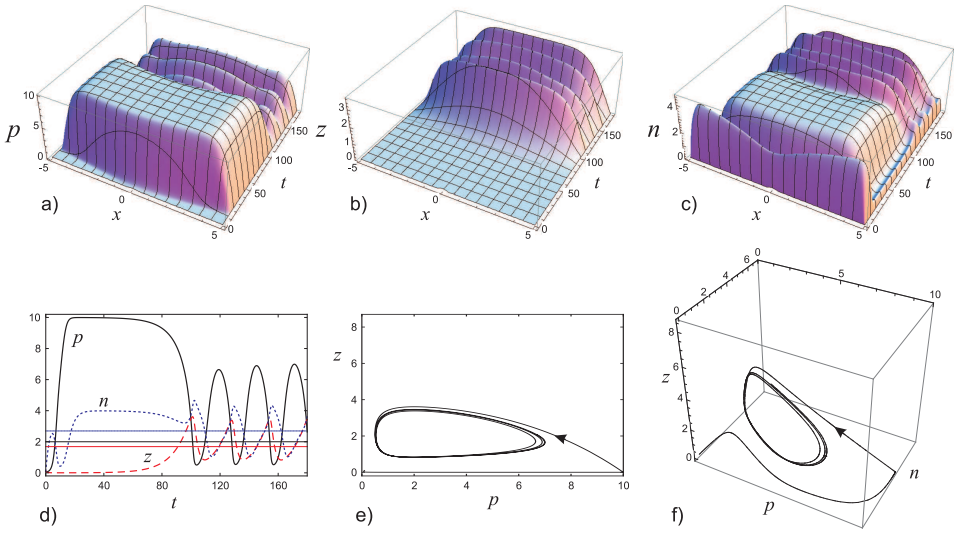

FIGURE 12. Transition from an empty region to a cyclic population state obtained for $a = 0.8$ where $\mathbf{U}_3^*$ is unstable. The quantities illustrated in the figures (a)-(f) are the same as the corresponding ones shown in Figure 10.

From the biological viewpoint, these results emphasize that the stability character of the NPZ system with respect to small perturbations is qualitatively similar to the PZ case. However, the limited availability of nutrient in the three-compartments model yields a slightly different behavior during the transient. Indeed, in the PZ system the phytoplankton bloom appears in very short times due to an unlimited

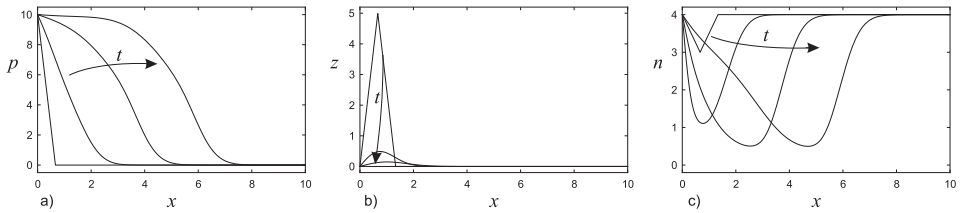

FIGURE 13. Numerical solutions of the system (12),(37),(38) connecting $\mathbf{U}_1^*$ and $\mathbf{U}_2^*$ at four different time instants: $t = 0, 5, 10, 15$. The parameters are the same as the ones used in Figure 9, together with $a = 1.2$.

availability of nutrient. On the contrary, in the NPZ model such a bloom is delayed since it requires, at first, the nutrient to grow from zero to a finite amount. The subsequent increase of phytoplankton induces a decrease of the nutrient and, once the phytoplankton has achieved its maximum, the nutrient and the zooplankton behave in a similar way as in the PZ model.

3.2. **Travelling waves.** Now, looking for travelling wave solutions admitted by the NPZ model, we obtain again the ODE's system (24), with $\mathbf{U}$, A and $\mathbf{B}$ given by (37), whose equilibria are exactly the same as the ones previously obtained (39). The linearization of such a system leads to the following characteristic equation for the eigenvalue λ:

$$\begin{aligned}
&\left[\left(\zeta'^* - V^2\right)\lambda^2 - \left(G_p^* - \tfrac{\zeta'^*}{d_p}\right)V\lambda + G_p^*\tfrac{\zeta'^*}{d_p}\right]\times\\
&\times\left[\left(\nu'^* - V^2\right)\lambda^2 - \left(h_n^* - \tfrac{\nu'^*}{d_n}\right)V\lambda + h_n^*\tfrac{\nu'^*}{d_n}\right]\times\\
&\times\left[\left(\chi'^* - V^2\right)\lambda^2 - \left(f_z^* - \tfrac{\chi'^*}{d_z}\right)V\lambda + f_z^*\tfrac{\chi'^*}{d_z}\right] +\\
&-\left(V\lambda - \tfrac{\zeta'^*}{d_p}\right)\left(V\lambda - \tfrac{\nu'^*}{d_n}\right)\left(V\lambda - \tfrac{\chi'^*}{d_z}\right)G_n^*h_z^*f_p^* +\\
&-\left(V\lambda - \tfrac{\zeta'^*}{d_p}\right)\left(V\lambda - \tfrac{\nu'^*}{d_n}\right)\left[\left(\chi'^* - V^2\right)\lambda^2 - \left(f_z^* - \tfrac{\chi'^*}{d_z}\right)V\lambda + f_z^*\tfrac{\chi'^*}{d_z}\right]h_p^*G_n^* +\\
&-\left(V\lambda - \tfrac{\zeta'^*}{d_p}\right)\left(-V\lambda + \tfrac{\chi'^*}{d_z}\right)\left[\left(\nu'^* - V^2\right)\lambda^2 - \left(h_n^* - \tfrac{\nu'^*}{d_n}\right)V\lambda + h_n^*\tfrac{\nu'^*}{d_n}\right]G_z^*f_p^* = 0.
\end{aligned} \tag{42}$$

The explicit expressions of the roots of (42), evaluated at the equilibria $\mathbf{U}_1^*$ and $\mathbf{U}_2^*$, are given by:

$$\begin{aligned}
\lambda_{1,2}(\mathbf{U}_1^*) &= \frac{V\left(\frac{n_0}{k+n_0} - \frac{\zeta'^*}{d_p}\right) \pm \left[V^2\left(\frac{n_0}{k+n_0} - \frac{\zeta'^*}{d_p}\right)^2 - 4\frac{\zeta'^*}{d_p}\frac{n_0}{k+n_0}\left(\zeta'^* - V^2\right)\right]^{\frac{1}{2}}}{2(\zeta'^* - V^2)}\\
\lambda_{3,4}(\mathbf{U}_1^*) &= \frac{-V\left(s + \frac{\nu'^*}{d_n}\right) \pm \left[V^2\left(s + \frac{\nu'^*}{d_n}\right)^2 + 4\frac{\nu'^*}{d_n}s\left(\nu'^* - V^2\right)\right]^{\frac{1}{2}}}{2(\nu'^* - V^2)}\\
\lambda_{5,6}(\mathbf{U}_1^*) &= \frac{-V\left(a\tilde{\alpha} + \frac{\chi'^*}{d_z}\right) \pm \left[V^2\left(a\tilde{\alpha} + \frac{\chi'^*}{d_z}\right)^2 + 4\frac{\chi'^*}{d_z}a\tilde{\alpha}\left(\chi'^* - V^2\right)\right]^{\frac{1}{2}}}{2(\chi'^* - V^2)}\\
\lambda_{1,2}(\mathbf{U}_2^*) &= \frac{-V\left(\frac{n_0}{k+n_0} + \frac{\zeta'^*}{d_p}\right) \pm \left[V^2\left(\frac{n_0}{k+n_0} + \frac{\zeta'^*}{d_p}\right)^2 + 4\frac{\zeta'^*}{d_p}\frac{n_0}{k+n_0}\left(\zeta'^* - V^2\right)\right]^{\frac{1}{2}}}{2(\zeta'^* - V^2)}
\end{aligned} \tag{43}$$

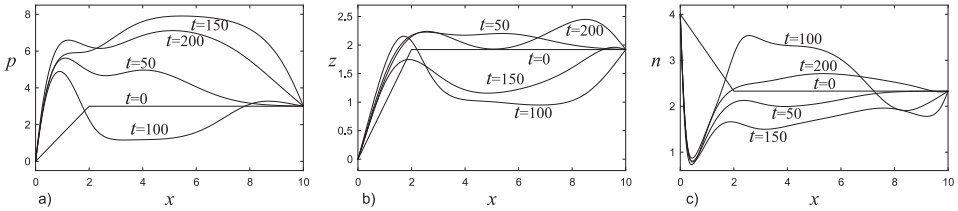

FIGURE 14. Numerical solutions of the system (12),(37),(38) connecting $\mathbf{U}_1^*$ and $\mathbf{U}_3^*$ at the indicated time instants for $a = 0.9$. The other parameters are the same as the ones used in Figure 9.

$$\lambda_{3,4}(\mathbf{U}_2^*) = \frac{-V\left(s+\frac{\nu'^*}{d_n}\right) \pm \left[V^2\left(s+\frac{\nu'^*}{d_n}\right)^2 + 4\frac{\nu'^*}{d_n}s\left(\nu'^* - V^2\right)\right]^{\frac{1}{2}}}{2(\nu'^* - V^2)}$$

$$\lambda_{5,6}(\mathbf{U}_2^*) = \frac{V\left(\tilde{\alpha}(a_{cr}-a)-\frac{\chi'^*}{d_z}\right) \pm \left[V^2\left((a_{cr}-a)-\frac{\chi'^*}{d_z}\right)^2 - 4\frac{\chi'^*}{d_z}\tilde{\alpha}(a_{cr}-a)\left(\chi'^* - V^2\right)\right]^{\frac{1}{2}}}{2(\chi'^* - V^2)}$$

which, accounting for the restriction arising from the hyperbolic nature of the model $V^2 < \min\{\zeta'^*, \chi'^*, \nu'^*\}$, point out that both equilibria are unstable since, for each state, two eigenvalues always exhibit positive real part.

On the other hand, the equation (42), evaluated at the equilibria $\mathbf{U}_3^*$, can be rewritten in the general form:

$$(V\lambda)^6 + b_1(V\lambda)^5 + b_2(V\lambda)^4 + b_3(V\lambda)^3 + b_4(V\lambda)^2 + b_5(V\lambda) + b_6 = 0 \qquad (44)$$

so that the character of the coexistence state depends on the sign of the coefficients b_i, $i = 1, 2, ..., 6$. In particular, as known from the Descartes' rule of signs, equation (44) admits at least one root with positive real part if at least one of the coefficients b_i is negative. By retaining the leading terms only, it is straightforward to ascertain that:

$$b_6 = -\frac{\nu'^*\zeta'^*\chi'^*}{d_n d_p d_z} a f_p^* \left(s + \alpha G_n^*\right) < 0 \qquad (45)$$

being $f_p^*\big|_{\mathbf{U}_3^*} > 0$ and $G_n^*\big|_{\mathbf{U}_3^*} > 0$, so that $\mathbf{U}_3^*$ is always unstable. Therefore, unlike the PZ model, travelling wave solutions cannot be observed in the NPZ system since all the equilibria are unstable.

Nevertheless, we perform some investigations in order to evaluate the possibility to establish connections between the steady states. In particular, we integrate numerically the system (12,37,38) in the spatial domain $0 \le x \le 10$ by fixing the equilibrium configurations at the considered computational boundaries. In such a numerical analysis we take into account the same previous set of parameters together with null initial fluxes. In detail, in Figure 13 the behavior of p, n and z at four different time instants is plotted by fixing the state $\mathbf{U}_2^*$ at the left boundary ($x = 0$) whereas $\mathbf{U}_1^*$ at the right one ($x = 10$). As it can be noticed, the system can evolve through a travelling wave-like path.

On the contrary, by setting $\mathbf{U}_1^*$ at $x = 0$ and $\mathbf{U}_3^*$ at $x = 10$ as boundary conditions, a possible connection between these steady states may exist even though such a solution deviates significantly away from a travelling wave-like profile, as shown in Figure 14.

This behavior is also represented in Figures 15 and 16 where the dynamics undergone by the three population densities is depicted in the time-spatial domain and in the phase space, respectively. In particular, it is possible to notice that the solution,

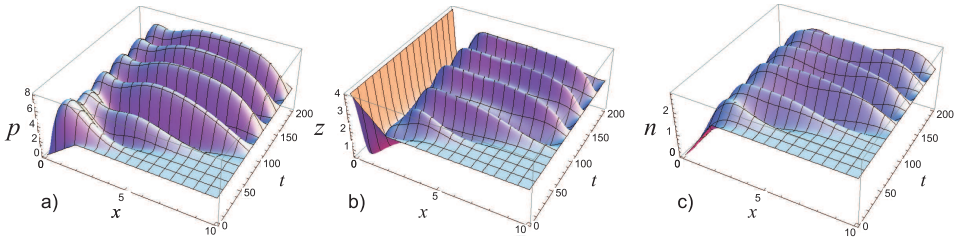

FIGURE 15. Dependence of the three population densities on time and space corresponding to the dynamics shown in Figure 14.

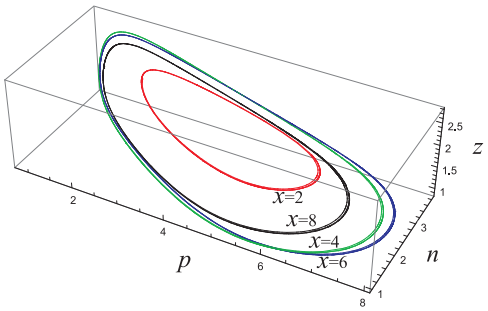

FIGURE 16. Phase portrait of nutrient, phytoplankton and zooplankton population for different spatial position. The figure exhibits limit cycles indicating oscillatory behavior. Parameter values are the same as Figure 14.

for a given spatial position, evolves in time along a limit cycle, whose amplitude depends on the position itself, as illustrated in Figure 16.

4. **Discussion.** Studies concerning the dynamics of plankton communities have been receiving a considerable attention not only from the marine ecology viewpoint but also for their crucial role played in climate dynamics.

In order to investigate the different scenarios connected to this ecological issue, many efforts have been devoted to develop mathematical models describing the interactions among the populations involved in an aquatic food chain.

In the present paper, along the leading ideas of the Extended Thermodynamic theory, we proposed hyperbolic reaction-diffusion models for a two or three compartments aquatic food chain.

Furthermore, we carried out a linear stability analysis around the corresponding steady states against uniform and non-uniform perturbations. Our analytical and numerical results revealed that the response of the ecosystem is not qualitatively different for the two models. From the biological point of view, it implies that the limited availability of nutrient does not alter significantly the stability character of the equilibria. On the other hand, from the mathematical point of view, the introduction of an additional state variable made the governing equations more complicated so that in the NPZ model some results were found numerically for a given set of parameters, differently from the PZ model where all the calculations were carried out analytically.

Then, we analyzed travelling waves as a mechanism by which the plankton communities may propagate into different environments. Owing to the hyperbolic structure of our models, such wave processes, unlike parabolic systems, take place at finite velocity, as desired. Investigations of the stability character of these solutions showed that the two proposed systems exhibit different behaviors. In fact, unlike the PZ model where the coexistence state is stable in given ranges of the control parameter, all the equilibria are unstable in the NPZ food chain. This means that the limited availability of nutrient fully destabilizes the system.

In particular, in spite of the instability of the two non-coexistence states ($\mathbf{U}_1^*$ and $\mathbf{U}_2^*$), we investigated on the possibility to link such equilibria. In the PZ model, the connection was established in virtue of the quasi-stability character of the trivial state, as shown in Fig.5. On the contrary, in the NPZ model, such a possibility was prevented due to the strong instability character of both states so that, in order to recover some additional information, we integrated the whole PDE system by setting these states as boundary values. As shown in Fig.13, after a transient, the system evolves through a travelling-wave-like path, similar to the one observed in the PZ model, thanks to the non-monotonic behavior exhibited by the nutrient (see Fig.13c). These results pointed out that, under such boundary conditions, phytoplankton can propagate as a wave and invade an empty region.

On the other hand, in a two-compartments system, a travelling wave connecting the coexistence state $\mathbf{U}_3^*$ and the trivial configuration $\mathbf{U}_1^*$ (or the zooplankton-free state $\mathbf{U}_2^*$) cannot exist due to the occurrence of an unstable limit cycle. Anyway, a possible connection between these steady states was achieved by considering non-null initial values of the dissipative fluxes, as shown in Fig.8. We stress that these results are strictly related to the assumption that the dissipative fluxes are independent variables (typical of Extended Thermodynamics) and cannot be observed in the corresponding parabolic models. Analogous results cannot be observed in the three-compartments system due to the instability of all steady states. However, by integrating numerically the whole PDE system where the unstable states are fixed at the boundaries, we found a non-monotonic and periodic behavior, as shown in Figs. 14-16. The results herein obtained thus confirmed that two and three compartments aquatic ecosystem models exhibit bifurcations and limit cycles for realistic values of parameters [8, 14, 18, 33].

Acknowledgments. This work was supported by INDAM-GNFM under the project entitled "Modelli matematici di interesse in biologia, ecologia e fluidodinamica: analisi qualitativa, studio della stabilita' e ricerca di soluzioni esatte"

REFERENCES

[1] M. Al-Ghoul and B. C. Eu, Hyperbolic reaction-diffusion equations and irreversible thermodynamics, *Physica D*, **90** (1996), 119–153.

[2] E. Barbera, C. Currò and G. Valenti, A hyperbolic reaction-diffusion model for the hantavirus infection, *Mathematical Methods in Applied Sciences*, **31** (2008), 481–499.

[3] E. Barbera, C. Currò and G. Valenti, A hyperbolic model for the effects of urbanization on air pollution, *Applied Mathematical Modelling*, **34** (2010), 2192–2202.

[4] E. Barbera, C. Currò and G. Valenti, Wave features of a hyperbolic prey–predator model, *Mathematical Methods in the Applied Sciences*, **33** (2010), 1504–1515.

[5] E. Barbera, G. Consolo and G. Valenti, Spread of infectious diseases in a hyperbolic reaction-diffusion susceptible-infected-removed model, *Physical Review E*, **88** (2013), 052719.

[6] K. Boushaba, O. Arino and A. Boussouar, A mathematical model for phytoplankton, *Mathematical Models and Methods in Applied Sciences*, **12** (2002), 871–901.

[7] S. J. Brentnall, K. J. Richards, J. Brindley and E. Murphy, Plankton patchiness and its effect on larger-scale productivity, *Journal of Plankton Research*, **25** (2003), 121–140.

[8] M. P. Cassinari, M. Groppi and C. Tebaldi, Effects of predation efficiencies on the dynamics of a tritrophic food chain, *Mathematical Biosciences and Engineering*, **4** (2007), 431–456.

[9] A. Chatterjee, S. Pal and S. Chatterjee, Bottom up and top down effect on toxin producing phytoplankton and its consequence on the formation of plankton bloom, *Applied Mathematics and Computation*, **218** (2011), 3387–3398.

[10] J. Chattopadhyay and S. Pal, Viral infection on phytoplankton-zooplankton system-a mathematical model, *Ecological Modelling*, **151** (2002), 15–28.

[11] C. Currò, D. Fusco and G. Valenti, Nonlinear wave analysis of a dissipative hyperbolic model of interest in biodynamics, *Far East Journal of Applied Mathematics*, **13** (2003), 195–215.

[12] S. R. Dumbar and H. G. Othmer, On a nonlinear hyperbolic equation describing transmission lines, cell movement, and branching random walks, in *Nonlinear Oscillations in Biology and Chemistry* (ed. H.G. Othmer), Lecture Notes in Biomathematics, Berlin, **66** (1986), 274–289.

[13] U. Ebert, M. Array, N. Temme, B. Sommeijer and J. Huisman, Critical Conditions for Phytoplankton Blooms, *Bulletin of Mathematical Biology*, **63** (2001), 1095–1124.

[14] A. M. Edwards and J. Brindley, Zooplankton mortality and the dynamical behaviour of plankton ecosystem models, *Bulletin of Mathematical Biology*, **61** (1999), 303–339.

[15] A. M. Edwards and A. Yool, The role of higher predation in plankton population models, *Journal of Plankton Research*, **22** (2000), 1085–1112.

[16] A. M. Edwards, Adding detritus to a nutrient-phytoplankton-zooplankton model: A dynamical systems approach, *Journal of Plankton Research*, **23** (2001), 389–413.

[17] J. Fort and V. Méndez, Wavefronts in time-delayed reaction-diffusion system. Theory and comparison to experiments, *Reports on Progress in Physics*, **65** (2002), 895–954.

[18] J. A. Freund, S. Mieruch, B. Scholze, K. Wiltshire and U. Feudel, Bloom dynamics in a seasonally forced phytoplankton-zooplankton model: Trigger mechanisms and timing effects, *Ecological complexity*, **3** (2006), 129–139.

[19] K. O. Friedrichs and P. D. Lax, System of Conservation Equation with a convex extension, *Proceedings of the National Academy of Sciences USA*, **68** (1971), 1686–1688.

[20] I. Koszalka, A. Bracco, C. Pasquero and A. Provenzale, Plankton cycles disguised by turbulent advection, *Theoretical Population Biology*, **72** (2007), 1–6.

[21] I. S. Liu, Method of Lagrange multipliers for exploitation of the entropy principle, *Archive for Rational Mechanics and Analysis*, **46** (1972), 131–148.

[22] H. Malchow, F. M. Hilker, R. R. Sarkar and K. Brauer, Spatiotemporal patterns in an excitable system with lysogenic viral infection, *Mathematical and Computer Modelling*, **42** (2005), 1035–1048.

[23] L. Matthews and J. Brindley, Patchiness in plankton populations, *Dynamics and Stability of Systems*, **12** (1997), 39–59.

[24] B. Mukhopadhyay and R. Bhattacharyya, Modelling phytoplankton allelopathy in a nutrient-plankton model with spatial heterogeneity, *Ecological modelling*, **198** (2006), 163–173.

[25] B. Mukhopadhyay and R. Bhattacharyya, Role of gestation delay in a plankton-fish model under stochastic fluctuations, *Mathematical Biosciences*, **215** (2008), 26–34.

[26] I. Müller and T. Ruggeri, *Rational Extended Thermodynamics*, Springer, New York, 1998.

[27] J. D. Murray, *Mathematical Biology I: An Introduction*, third ed., Springer, Berlin, 2002.

[28] A. Palumbo and G. Valenti, A mathematical model for a spatial predator-prey interaction, *Mathematical Methods in the Applied Sciences*, **25** (2002), 945–954.

[29] J. H. Steele and E. W. Henderson, A simple plankton model, *The American Naturalist*, **117** (1981), 676–691.

[30] J. H. Steele and E. W. Henderson, The role of predation in plankton models, *Journal of Plankton Research*, **14** (1992), 157–172.

[31] J. E. Truscott and J. Brindley, Ocean plankton populations as excitable media, *Bulletin of Mathematical Biology*, **56** (1994), 981–998.

[32] J. E. Truscott and J. Brindley, Equilibria, Stability and Excitability in a General Class of Plankton Population Models, *Philosophical Transactions: Physical Sciences and Engineering, Nonlinear Phenomena in Excitable Media*, **347** (1994), 703–718.

[33] R. K. Upadhyay, W. Wang and N. K. Thakur, Spatiotemporal dynamics in a spatial plankton system, *The Mathematical Modelling of Natural Phenomena*, **5** (2010), 102–122.

Received February 18, 2014; Accepted November 04, 2014.

E-mail address: ebarbera@unime.it
E-mail address: gconsolo@unime.it
E-mail address: gvalenti@unime.it